Available online at www.sciencedirect.com
ScienceDirect
Journal of Nuclear Materials 363–365 (2007) 162–166
journal of nuclear materials
www.elsevier.com/locate/jnucmat

B2/Eirene modeling of EAST divertor target power loading with enhanced wall carbon source and additional neon injection

H.Y. Guo [a,b,*], S. Zhu [a], J. Li [a]

[a] Institute of Plasma Physics, Chinese Academy of Sciences, Hefei, China
[b] Redmond Plasma Physics Laboratory, University of Washington, Seattle, USA

Abstract

A major concern for EAST and future high-powered steady-state machines such as ITER is the power handling capability of the divertor target plates. Detailed modeling using the B2/Eirene code is carried out to assess the target power loading of the EAST divertor with both single-null and double-null configurations. A remarkable output is that an enhanced wall carbon source from chemical sputtering may lead to strong radiation in the plasma boundary, significantly reducing heat fluxes to the target plates, with little contamination to the core plasma at sufficiently high densities due to strong divertor screening. As a means of further reducing the power fluxes to the target plates and actively controlling the inner/outer divertor asymmetry in power loading, localized neon gas puffing from the outer divertor is investigated using B2/Eirene. The effect of this highly radiating impurity on target power loading and the consequence for core contamination is also presented.
© 2007 Elsevier B.V. All rights reserved.

PACS: 52.55.Rk; 52.25.Vy; 52.40.Hf; 52.65.Pp

Keywords: EAST; B2/Eirene; Divertor power load; Chemical sputtering; Neon puffing

1. Introduction

The experimental advanced superconducting tokamak (EAST) is a fully superconducting tokamak presently being built in China to achieve steady-state operation with electron temperature $T_e > 10$ keV, and electron density $n_e > 10^{20}$ m^{-3}. Up to 1 MA of plasma current will be driven and sustained over 1000 s by lower hybrid waves. The principal mission of EAST is to integrate high fusion performance and steady-state operation to establish the scientific and technological bases for the next step burning plasma devices, such as ITER.

Power handling is a great challenge for operating a high-powered steady-state machine. The engineering design for EAST requires that the maximum power flux to the target plates during the first phase of operation is below 1 MW/m^2 to ensure long pulse (>100 s) operation [1]. Thus, a large portion of the power flow into the scrape-off-layer (SOL) from the

* Corresponding author. Address: Redmond Plasma Physics Laboratory, University of Washington, 14700 NE 95th Street, Suite 100, Redmond, WA 98052, USA.
E-mail addresses: hguo@aa.washington.edu (H.Y. Guo), szhu@ipp.ac.cn (S. Zhu).

0022-3115/$ - see front matter © 2007 Elsevier B.V. All rights reserved.
doi:10.1016/j.jnucmat.2007.01.012

confined core plasma must be lost by radiation and charge-exchange before reaching the target plates. This dictates that EAST must be operated close to conditions of plasma detachment. EAST has adopted ITER-like vertical target configuration with tightly fitted side baffles and a central dome in the private region to separate physically the inner and outer divertors and to minimize the leakage of neutrals to the main plasma. With this configuration, most of the particle flux incident on the target plates is re-emitted towards the separatrix, below the X-point. These recycling particles are ionized near the separatrix, thus decreasing temperature and increasing density in its vicinity. As a result, the peak heat flux is reduced and the profile is broadened near the separatrix, thus reducing target power loading [2,3]. In addition, the preferential ionization of the recycling neutrals near the separatrix facilitates plasma detachment at the separatrix, i.e., partial detachment, at a lower main plasma density [4], which is desired for lower hybrid current drive (LHCD) in EAST.

In this paper, we present detailed modeling studies of the divertor target power loading in EAST with various intrinsic carbon sources and external neon puffing, as well as the divertor screening for these impurities, using the B2/Eirene code package, SOLPS Version 4.0 [5]. In Section 2 we describe the EAST divertor geometry and modeling parameters for SOLPS 4.0. In Section 3 we report the performance of the EAST divertor with the basic single-null configuration in terms of divertor target power loading and contamination from the intrinsic carbon impurity assuming various chemical sputtering conditions. Comparisons are made with the connected double-null (CDN) divertor configuration in Section 4. Preliminary results on additional neon puffing are presented in Section 5, followed by a summary in Section 6.

2. EAST divertor geometry and model assumptions

EAST has a flexible poloidal field control system to accommodate both single-null (SN) and double-null (DN) divertor configurations. Fig. 1 shows the divertor geometry of EAST with the SN and CDN configurations. The major parameters for the two divertor configurations are listed in Table 1. The magnetic equilibriums of EAST are generated using the EFIT code and are the basis of the numerical grid generation for the SOLPS 4.0. The SOLPS 4.0-B2/Eirene code package consists of a multi-fluid code B2 for electrons and ions at each ionization state, coupled to a Monte-Carlo code Eirene for neutrals. The deuterium ion density n_D and the power flux P_s at the core-edge boundary are used as the major input parameters to the code. A total heat flux $P_s = 4$ MW is chosen in the simulation to represent typical projected operating conditions in EAST in the first phase of operation with a total heating power of 10 MW. P_s is then equally split between the electron and ion channels. n_D is varied systematically in the simulation to reproduce various operating conditions. The recycling coefficient for deuterium is set to unity at the divertor target plates and the main chamber wall for the envisaged long pulse operation in EAST. The anomalous cross-field transport diffusivity, $D_\perp = 0.3\ m^2\ s^{-1}$, and the anomalous cross-field ion and electron heat diffusivities, $\chi_i = \chi_e = 1.0\ m^2\ s^{-1}$. The parallel plasma transport is flux limited, and no drifts are present in the simulation.

The carbon sources at the wall and the divertor target plates are computed assuming both physical

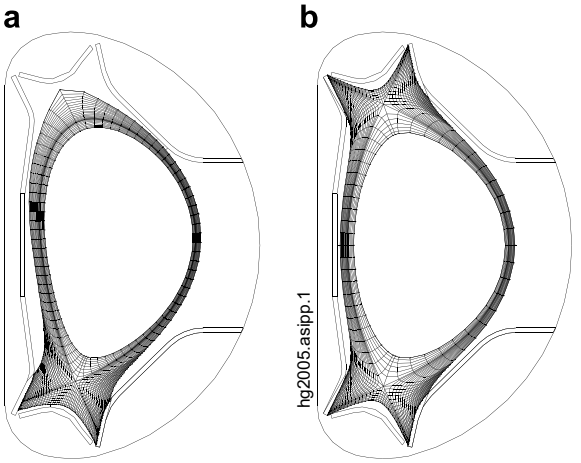

Fig. 1. Schematic of EAST divertor geometry with two different configurations: (a) single-null (SN), (b) connected double-null (CDN).

Table 1
Major parameters of EAST with two different divertor configurations, i.e., single-null (SN) and connected double-null (CDN)

	SN	CDN
Major radius, R (m)	1.94	1.94
Minor radius, a (m)	0.46	0.47
Elongation at separatrix, κ_x	1.69	1.76
Upper triangularity at separatrix, δ_{xu}	0.32	0.56
Lower triangularity at separatrix, δ_{xl}	0.54	0.56
Plasma volume, V_p (m^{-3})	11.9	12.5

sputtering and chemical sputtering. The physically sputtered impurities are assumed to have a Thompson velocity distribution. The chemically sputtered atoms are given an energy of 0.5 eV, as would be expected from simple molecular break-up of methane [6]. The actual chemical sputtering processes are very complex, and cannot be fully modeled using SOLPS 4.0. In this simulation, we have used a fixed chemical sputtering yield based on the recently published chemical sputtering data compiled by Roth et al. [7].

3. Effect of enhanced wall carbon source

To investigate the basic divertor performance with only the intrinsic carbon impurity, we have carried out a density scan ranging from attached to fully detached plasma conditions for the ITER-like SN divertor configuration, as shown in Fig. 1(a), with the following impurity sources:

- Physical sputtering plus chemical sputtering with a fixed yield, $Y_{ch} = 2\%$, at all the material surfaces including the divertor target plates and the main chamber wall, which is a typical value for the divertor plasma conditions in the present machines.
- Physical sputtering plus chemical sputtering with $Y_{ch} = 2\%$ at the target plates, but with an enhanced yield, $Y_{ch} = 8\%$, at the rest of the material surfaces including the main chamber wall to allow for the flux dependence reported in [7], and any changes in the surface structure of the deposits.

Fig. 2 shows the B2/Eirene predictions of the calculated peak heat fluxes to the outer target plate, $q_{pk,out}$, and the inner target plate, $q_{pk,inn}$, as well as Z_{eff} at the separatrix evaluated at the outer midplane, Z_s, as a function of the electron density at the outer midplane separatrix, n_s, with the different chemical sputtering assumptions. The dashed line indicates the upper density limit for LHCD in EAST. As can be seen, the peak heat fluxes to both outer and inner divertor target plates are reduced for the case with $Y_{ch} = 8\%$ at the wall, with a more pronounced reduction at the inner target plate. With this enhanced wall carbon source, plasma detachment occurs at a lower density, as indicated by a sudden reduction in the peak heat fluxes at $n_s \sim 1.7 \times 10^{19}$ m^{-3}. As a result, the peak heat fluxes

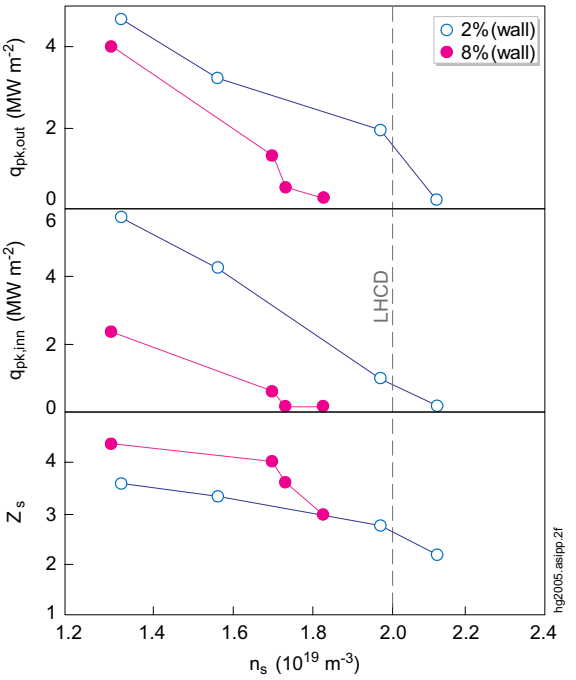

Fig. 2. Peak heat fluxes to the outer target plate, $q_{pk,out}$, and the inner target plate, $q_{pk,inn}$, together with the edge carbon content, Z_s, as a function of the edge electron density, n_s, predicted by B2/Eirene with the power fluxes across the core-edge boundary, $P_s = 4$ MW for an ITER-like SN divertor configuration with different carbon wall sources. The upper density limit for LHCD is also indicated.

to the target plates are significantly reduced at the densities desired for LHCD.

As expected, the edge impurity content Z_s decreases as n_s increases, due to improved divertor screening, which is presumably ascribable to a stronger role for plasma friction and a weaker role for the thermal force. At a given density, divertor screening is stronger for impurities produced by chemical sputtering than for those from physical sputtering, because chemically produced impurities have a much lower energy. It appears that increasing the chemical sputtering yield at the wall from 2% to 8% leads to higher carbon concentrations at low densities. However, at sufficiently high densities, i.e., close to plasma detachment, Z_s decreases rapidly for the enhanced wall source case, down to similar values to those for the case with the lower wall source.

4. Comparison between SN and CDN configurations

One of the considerations of going from a single-null to a double-null divertor configuration is to

distribute the output power more widely and, in particular, to reduce the peak power flux to the target plates. To investigate target power loading in the projected double-null discharges in EAST, we have used the same modeling inputs to the B2/Eirene code package as for the single-null divertor configuration except that the total power flux across the core-edge interface, P_s, is split between the outboard and the inboard SOLs with a ratio of $P_{s,out}/P_{s,inn} = 3$, in consideration of the geometric effects. Fig. 3 compares the peak heat fluxes at the outer and inner divertor target plates and the edge impurity content between the SN and CDN divertor configurations, assuming $Y_{ch} = 2\%$ at all the material surfaces for both cases. As can be seen, the peak heat fluxes are reduced at both outer and inner target plates for the CDN configuration, as expected. Z_s is also significantly reduced. However, in contrast to SN operation where both inner and outer divertor plasmas approach the detached state at similar n_s, plasma detachment starts at a much lower density at the inner targets than at the outer targets for the CDN configuration. Full plasma detachment at the inner target plates may lead to confinement degradation due to excessive neutral influxes around the X-point to the core. Therefore, in the double-null operation, the range of operating densities may be reduced. Moreover, in this case, most of the outer divertor plasmas remain partially attached, with substantial power flux going to the outer target plates, which is undesirable for long pulse operation.

5. Effect of neon puffing

To further reduce divertor target power loading and the inner/outer asymmetry, localized Ne puffing from the *outer* lower divertor slot is simulated for the CDN configuration with a puff rate of $10^{20}\ s^{-1}$, and $Y_{ch} = 2\%$ for all the material surfaces including the divertor targets and the wall surfaces. At sufficiently high densities, Ne is well restricted to the vicinity of the lower divertor due to strong divertor/SOL screening. However, significant radiation from neon is also present in the inner lower divertor, presumably due to the leakage of neon directly through the private region or around the

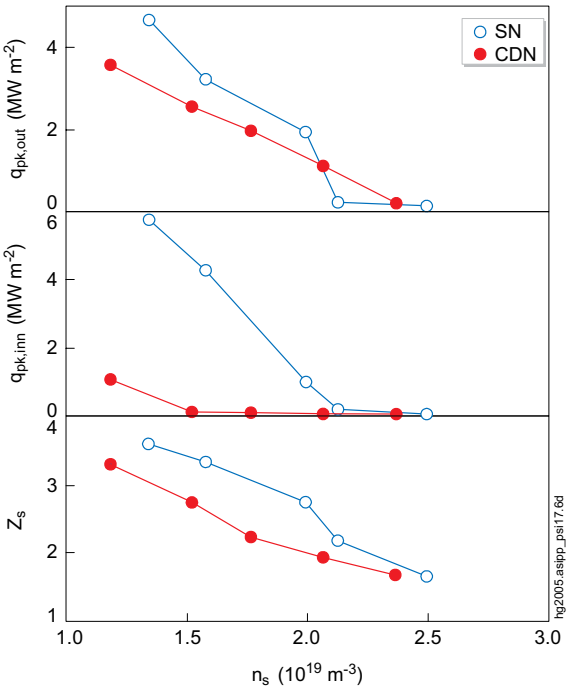

Fig. 3. Comparison of the peak heat fluxes to the outer and inner target plates, $q_{pk,out}$ and $q_{pk,inn}$, as well as the edge impurity content, Z_s, between SN and CDN, assuming $Y_{ch} = 2\%$ at all the surfaces.

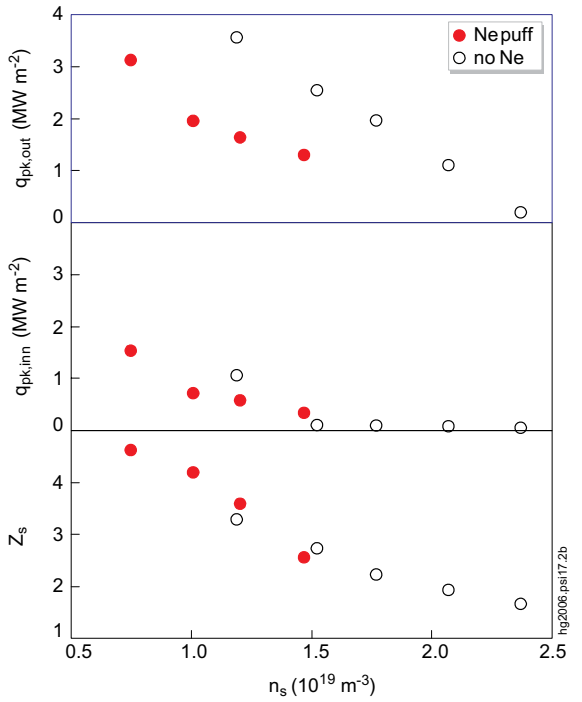

Fig. 4. Comparison of the peak heat fluxes to the outer and inner target plates, $q_{pk,out}$ and $q_{pk,inn}$, as well as the edge impurity content, Z_s, between the cases with and without neon puffing for the CDN configuration with $P_s = 4$ MW and with a fixed chemical yield of 2% for carbon.

X-point. Nevertheless, Ne puffing from the outer divertor dramatically reduces the heat fluxes to the outer divertor target plates, mitigating the degree of the inner/outer divertor asymmetry. To illustrate this, Fig. 4 compares the peak heat fluxes to the outer and inner target plates, $q_{pk,out}$ and $q_{pk,inn}$, together with the edge impurity content Z_s between the cases with additional neon puffing and those with only the intrinsic carbon impurity present in the plasma. It is remarkable that neon puffing does not appear to affect much the edge impurity content, suggesting very strong divertor screening for neon under these modeled conditions.

The inner/outer asymmetry in power loading may be further improved by optimizing the neon puffing location to maximize Ne ionization inside the outer divertor plasma. In addition, physically isolating the inner and outer divertors using a septum may help preventing the direct leakage of neon from the outboard divertor into the inboard region.

6. Summary

We have used the SOLPS 4.0-B2/Eirene code package to assess divertor target power loading and impurity contamination for EAST with varying intrinsic carbon sources and external neon puffing. Based on the newly established flux dependence of carbon chemical sputtering yields, we have introduced an enhanced carbon source at the wall surface with a yield up to 8%. It appears that the enhanced wall chemical source leads to strong radiation in the plasma boundary, significantly reducing the power fluxes to the divertor target plates and promoting plasma detachment at a lower density, which is desired for LHCD in EAST. At sufficiently high densities, the impurity content remains largely unchanged because of strong divertor screening for the chemically produced impurities, which have a much lower energy than those produced by physical sputtering. The peak heat fluxes to the target plates can be further reduced by operating with the double-null divertor configuration, accompanied by a significant reduction in the impurity concentration at the edge. However, the double-null operation leads to a stronger divertor asymmetry in target power loading, favoring the outer target plates, since only a small share of the power flux across the separatrix reaches the inner divertor. Localized neon puffing from the outer divertor dramatically reduces the peak heat fluxes to the outer divertor target plates and appears to provide an effective means to mitigate the degree of the inner/outer divertor asymmetry in power loading. Furthermore, the impurity content at the separatrix remains nearly the same with Ne puffing, suggesting very strong divertor screening for neon.

Acknowledgements

The authors would like to thank D. Coster and A.S. Kukushkin for help with the initial setup for the modeling of neon puffing, and support from the Center for Computational Science, Hefei Institutes of Physical Sciences. H.Y. Guo gratefully acknowledges the support of K.C. Wong Education Foundation, Hong Kong.

References

[1] D.M Yao, private communications.
[2] S. Zhu, Contrib. Plasm. Phys. 40 (2000) 322.
[3] S. Zhu, X. Zha, J. Nucl. Mater. 313–316 (2003) 1020.
[4] A. Loarte, Plasma Phys. Control. Fus., 43 (2001) R183.
[5] D.P. Coster, X. Bonnin, B. Braams et al., in: Proceeding 19th IAEA Fusion Energy Conference, Lyon, 2002, Paper TH/P2-13.
[6] P.C. Stangeby et al., J. Nucl. Mater., these Proceedings, doi:10.1016/j.jnucmat.2007.01.008.
[7] J. Roth, R. Preuss, W. Bohmeyer, et al., Nucl. Fusion 44 (2004) L21.